Letter

Photocurrent-Detected 2D Electronic Spectroscopy Reveals Ultrafast Hole Transfer in Operating PM6/Y6 Organic Solar Cells

Luca Bolzonello,* Francisco Bernal-Texca, Luis G. Gerling, Jana Ockova, Elisabetta Collini, Jordi Martorell, and Niek F. van Hulst*

Read Online

ACCESS | Metrics & More | Article Recommendations | Supporting Information

ABSTRACT: The performance of nonfullerene-acceptor-(NFA)-based organic solar cells is rapidly approaching the efficiency of inorganic cells. The chemical versatility of NFAs extends the light-harvesting range to the infrared, while preserving a considerably high open-circuit-voltage, crucial to achieve power-conversion efficiencies >17%. Such low voltage losses in the charge separation process have been attributed to a low-driving-force and efficient exciton dissociation. Here, we address the nature of the subpicosecond dynamics of electron/hole transfer in PM6/Y6 solar cells. While previous reports focused on active layers only, we developed a photocurrent-detected two-dimensional spectroscopy to follow the charge transfer in fully operating devices. Our measurements reveal an efficient hole-transfer from the Y6-acceptor to the PM6-donor on the subpicosecond time scale. On the contrary, at the same time scale, no electron-transfer is seen from the donor to the acceptor. These findings, putting ultrafast spectroscopy in action on operating optoelectronic devices, provide insight for further enhancing NFA solar cell performance.
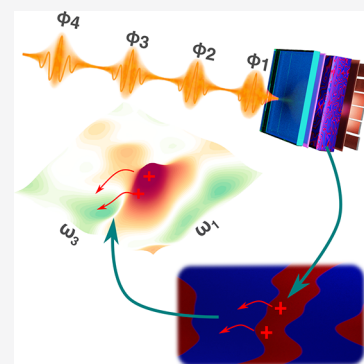
The introduction of two-dimensional electronic spectroscopy (2DES) has spurred the study of ultrafast dynamics and state-to-state energy transfer.[1] Specifically, 2DES has fully proved its potential to uncover the transfer path involved in complex photophysical systems (e.g., light-harvesting complexes,[2−4] quantum dots,[5] molecular aggregates,[6] excitonic dimers[7]). Over the past decade, different implementations of 2DES have been proposed, each with distinct advantages and disadvantages.[8] On the one hand, in conventional box-car-type 2DES, the signal is collected as a third order polarization signal, which propagates in a specific phase matching direction. Although this approach enables background free detection of the weak nonlinear response, it is limited to large macroscopic interaction volumes. On the other hand, the fully collinear geometry allows overcoming this issue, by exploiting phase cycling to extract components of the third order polarization from the detected fourth order population.[9] The collinear alternative allows reducing the interaction volume (using high NA objectives) and moreover enables the combination of 2DES with other spectroscopic techniques. Indeed, the detection is not limited to the nonlinear polarization, i.e., coherent light emitted, but potentially extends to any kind of observable proportional to population conditions after the 4-pulse excitation, for example, fluorescence[10] or current,[11,12] but even photoions[13] and photoelectrons.[14] The correlation with additional observables holds great promises to expand the range of physical problems tackled by 2DES. For instance, local microscopic 2DES using fluorescence detection has been demonstrated by Ogilvie and Brixner groups.[15,16] Photocurrent detected ultrafast spectroscopy has several advantages of sensitivity, selectivity, and resolution with respect to all-optical measurements as recently described by the Vella group.[17]

A natural application of photocurrent-detected ultrafast spectroscopies is the study of the photophysics of donor and acceptor blends in organic solar cells (OSC). Ultrafast dynamics in OSC is much more diversified relative to semiconductors like silicon. Indeed, inside silicon, the dielectric constant is huge, so the photogenerated electrons and holes pairs display a low binding energy making charge separation not a critical step for photovoltaic efficiency.[18] On the contrary, electrons and holes generated in organic materials are initially strongly bound in molecular excitons. Their dissociation requires a spacing between the HOMO and LUMO energy levels of the donor and the acceptor with the aim of driving charge separation and subsequent transfer between the two materials. This driving force is necessary to enhance charge transfer and thus current amplitude; however, this is at the cost of lowering the effective voltage, reducing the overall efficiency of the cell. In OSC then, the efficiency of charge transfer between different moieties acquires a crucial importance. Recently, a new kind of material was introduced: the nonfullerene acceptors (NFA). In these new materials,
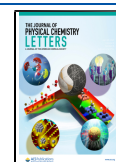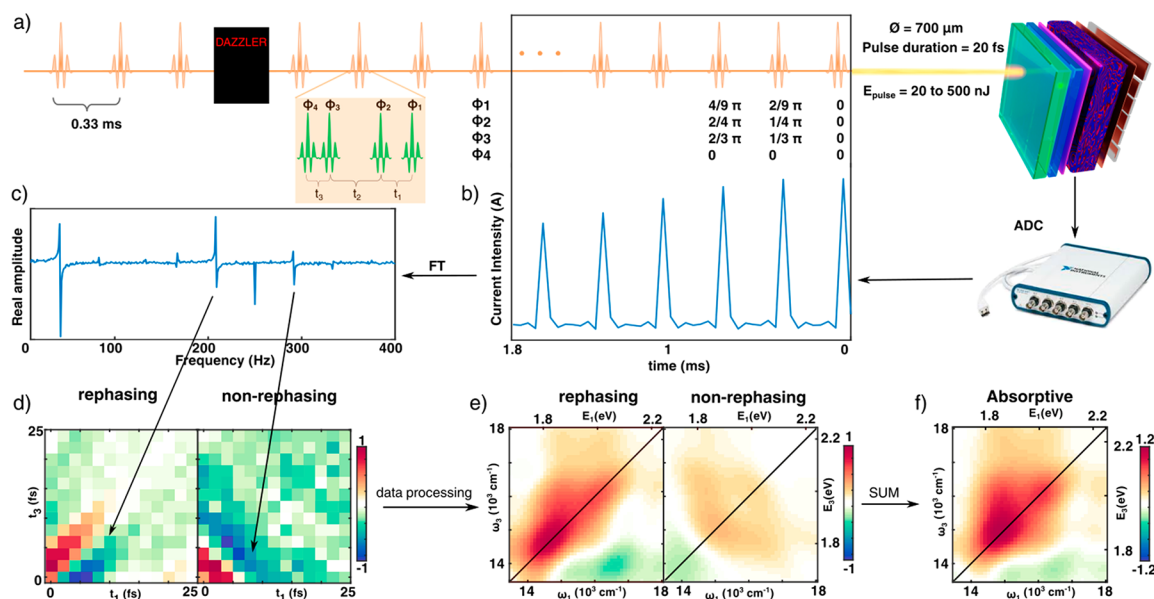
Figure 1. (a) Pulse-by-pulse phase modulation scheme: the pulses of a 3 kHz amplified Ti:Sa laser, after going through a NOPA and prism compressor, are shaped by Dazzler. The shaping is made such that from one laser pulse 4 delay- and phase-controlled pulses are generated. At every following laser pulse a phase delay is introduced in 3 of the 4 generated pulses such that their phases are modulated with different frequencies. Laser pulses illuminate the photovoltaic cell that generates a current/voltage signal, read-out by a National Instruments card. This allows to retrieve a modulated signal (b) of which the FFT spectrum (c) gives the components of the 4th order population at different frequencies. (d) The 2DES maps are rebuilt by extracting the components at all time-delays. After data processing and Fourier transform along t_1 and t_3, (e) the standard rephasing and non rephasing maps are obtained and (f) the sum of these give the absorptive maps.

there is evidence showing that the driving force is not a constraint for efficient charge separation.[19,20] Recent density functional theory studies to calculate exciton binding energies in the NFA domain indicate that an efficient molecular orbital delocalization may be the key to allow a low-driving-force efficient exciton dissociation.[21] Avoiding the intrinsic voltage loss typical of Fullerene based acceptor may significantly contribute to the recent boosting of OSCs power conversion efficiency (PCE).

Y6 (also known as BTP-4F) is a n-type NFA, synthesized for the first time by Zou's group,[22] that stands among other fused-ring NFA's showing features such as high electron mobility and a red-shifted absorption up to 800 nm. When blended with p-type polymer donor PM6 (also known as PBDB-T-2F), the resulting PM6:Y6 based OSCs have achieved a notorious breakthrough in efficiency: PCE of 15.7%.[23−25] This system exhibits a remarkably high current density due to the complementary donor and acceptor absorption and low driving forces resulting in a relatively reduced energy loss ($E_{loss} \sim 0.55$ eV), estimated from the difference between the bulk heterojunction (BHJ) optical band gap and the V_{oc}.[26] Currently, the Y6-based devices or its derivatives as electron acceptors provide the highest PCEs among all binary OSCs.[27]

To further increase the PCE, a detailed understanding of the fundamental charge generation processes is needed. While it is established that the improved band alignment of donor and acceptors is beneficial, the underlying mechanism leading to such high efficiencies is yet to be understood. While many recent works mostly focused on energy levels, donor/acceptor component ratio, and nanomorphology,[28,29] the ultrafast dynamics has been demonstrated to play a role.[30−32]

Here, we present a novel and effective photocurrent-detected collinear 2DES (pc-2DES) scheme, which resolves the ultrafast dynamics of charge separation directly on an operating solar cell, without any need of preliminary sample preparation and avoiding hard transmitted light detection, while collecting the full excited state dynamics by effective pulse-by-pulse shaping with simple collinear laser setup.

The pc-2DES is particularly suitable for characterization of such OSC dynamics for different reasons: (i) low repetition rate laser (0.33 ms between subsequent laser pulses), which allow the system to discharge and recover completely between pulses; (ii) high pulse delay accuracy (sub fs), for precise 2DES signal reconstruction; (iii) intrinsic phase locked pulses, which preserve the final map shape; and (iv) the use of broadband pulses, simultaneously covering the spectral features of the different moieties both in excitation and detection.

The core of our technique is the generation of 4 collinear pulses and the precise control of their mutual delays and phases. Although this configuration could be realized by using a multibranch interferometric setup,[10] the use of a suitable pulse shaper affords higher flexibility.[16,33,34] To retrieve all the components of the fourth order population, phase cycling is needed, and, in particular, it requires at least 27 steps.[35] This means that in a measurement, for any set of time delays (t_1, t_2, t_3), 27 sets of phases have to be collected, which would make the measurement long and very sensitive to laser fluctuations. Depending on the kind of laser, different approaches can overcome these issues: using oscillators, with MHz rep rate, it is possible to use phase modulation that extracts the signal, while retrieving the components demodulating the signal at specific combination frequencies;[12,15] using amplified Ti:Sa lasers and an acousto-optic pulse shaper, one can exploit pulse by pulse shaping to speed up the measurement.[34] Because of different pulse energies and repetitions rates, the first scheme is more suitable for microscopy application with fluorescence detection, while the second is more suitable for ensemble and slow recombination samples. Here, we present a photocurrent-

3984
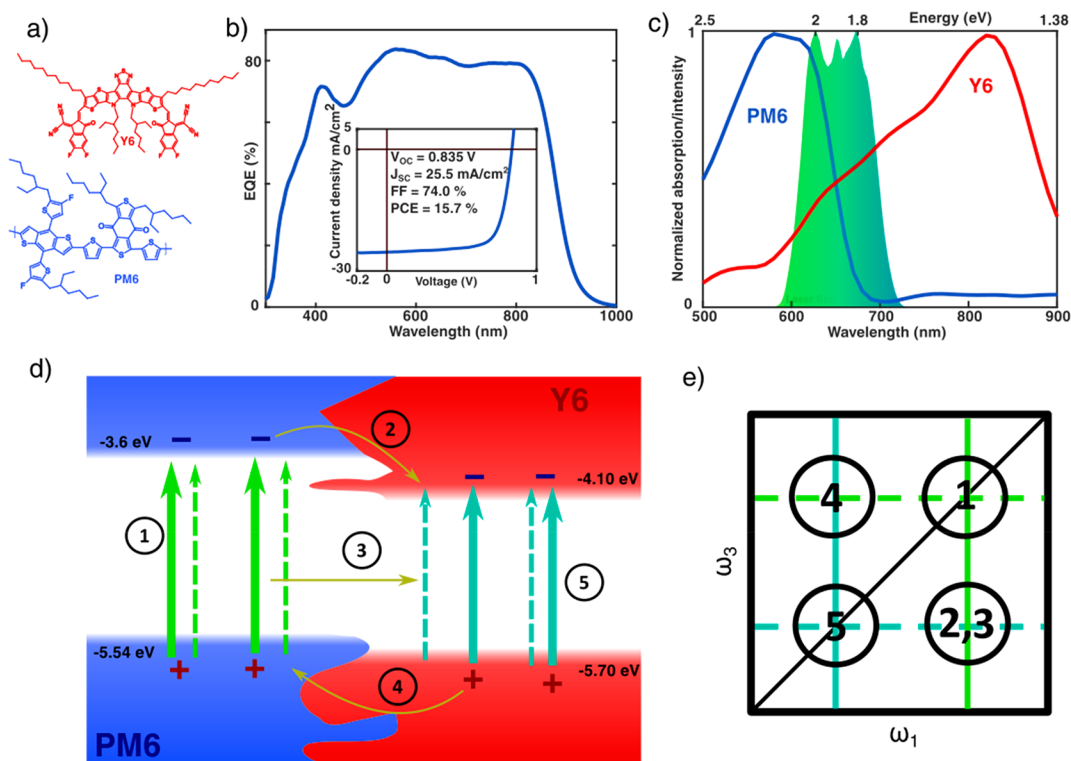
Figure 2. (a) Molecular structures of PM6 and Y6. (b) EQE spectrum of the cell, with value close to 80% in visible and NIR ranges. (c) Normalized absorption spectra of single components compared with the laser spectrum. (d) Pictorial representation of the BHJ layer made of PM6 and Y6. The various processes that occur within ultrafast range associated excitation-detection transitions are illustrated. (e) 2DES coordinates of these combination. Numbers 1 and 5 represent GSB for the same transition, for example, when the excitation happens within a moiety. Numbers 2, 3, and 4 represent the possible mechanism at interface, electron, and exciton transfer from PM6 to Y6 and the hole transfer from Y6 to PM6, respectively. If after excitation (bold lines), a transfer occurs between the materials, the GSB will be detected by the transition in the other material (dashed lines) and visualized at cross-peaks in the 2DES map.

detected setup which combines the advantages of both approaches, pulse-by-pulse shaping while modulating the phases of the different pulses.

Our pulse-by-pulse phase modulation scheme is shown in Figure 1a. We use a 3 kHz Ti:Sa amplified laser (Coherent Libra), which pumps a home-modified noncollinear optical parametric amplifier (TOPAS white). After a prism compression stage, the beam passes through an acousto-optic pulse shaper (Fastlite Dazzler) that from each pulse generates a set of 4 time-delayed pulses. Through the streaming option of the Dazzler it is possible to upload to a fast memory tens of different shapes that are, one by one, streamed each time a pulse passes through the Dazzler. This pattern is repeated many times. To have a convenient modulation, it is sufficient to vary the phases of different pulses within this recurrent pattern such that the phase of the first pulse is 0 and the last is a 2π multiple minus one step (Figure 1b). This pulse-by-pulse phase shaping speeds up the measurement, with all the phases of the pulses automatically locked, and allows for cleaning the data through an intrinsic digital lock-in detection. The beam is focused to a beam waist of 700 μm, on the 0.06 cm^2 photovoltaic cell, and the photocurrent is read-out through a National Instruments board (NI usb-4432). The collected macroscopic time-signal (Figure 1c) is Fourier transformed to extract the frequencies corresponding to the 2DES response[36] (see Figure 1d), such as rephasing and nonrephasing components. A scan of all different time-delays between the shaped pulses gives the full time-dependent fourth order signal $S(t_1, t_2, t_3)$ (Figure 1e), which is transformed in frequency domain $S(\omega_1, t_2, \omega_3)$, to display the energy maps typical for 2DES spectroscopy. Rephasing and nonrephasing signals can be summed, thereby giving access to the absorptive part of the fourth order signal (Figure 1f). This absorptive signal carries components which can be directly identified with those observed in a standard pump−probe experiments, e.g., ground state bleaching (GSB) and stimulated emission (SE) as positive signals and excited state absorption (ESA) as negative one.[9,12] In other words, absorptive maps contain the full picture of the excited state dynamics. The measurements were performed at 15 μJ/cm^2 which turned out a good compromise to operate in the nonlinear regime, with sufficient S/N, while avoiding higher order artifacts (see S6 in SI).

Although the phase modulation approach is an effective way of recording 2DES data, pulse-by-pulse shaping capabilities can possibly lead to other efficient approaches. For instance, the group of Brixner proposed an acquisition routine for fluorescence detected 2DES[34] in which each pulse corresponds to a different set of delays and phase, being able to complete in the shortest time all the sets necessary to construct the fourth order signal, including the 27 phase cycling step. Hence, the entire signal could potentially be acquired in minutes, while avoiding laser instability issues, even in the case of averaging. However, in the case of photocurrent detection in photovoltaic devices, absolute voltage instabilities on short time scales (e.g., from space charge formation, ion migration, and shunt currents) generate a fluctuating background which complicates the slow phase cycling. Therefore, the quality of the final signal
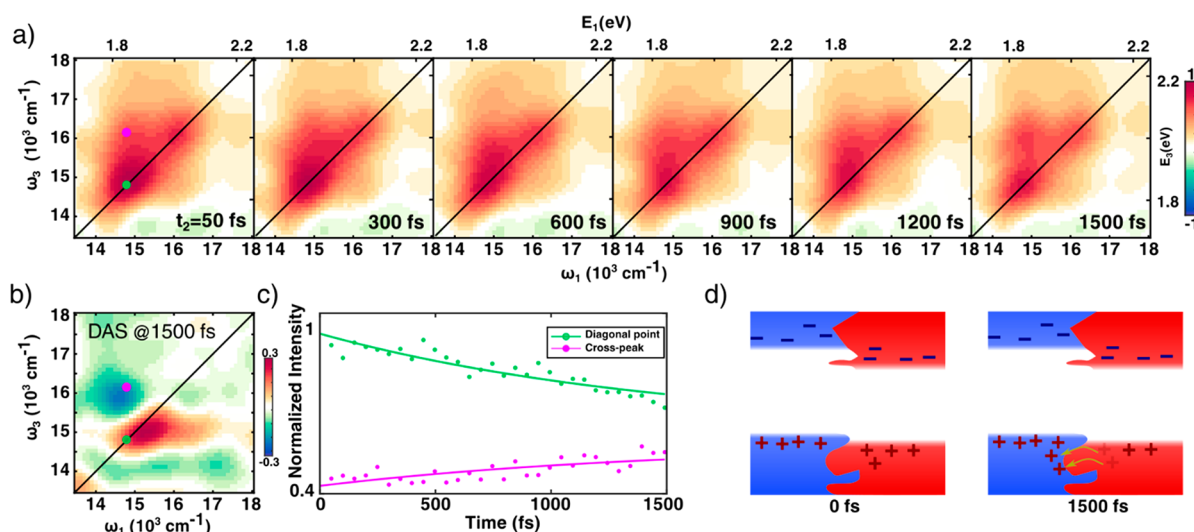
Figure 3. (a) Evolution of absorptive 2DES maps between 50 and 1500 fs. (b) Decay associated map associated with 1500 fs decay. Positive and negative amplitude are associated with decreasing and increasing signal, respectively. (c) Population time evolutions of diagonal- and cross-peak plotted with their global fitting curves. (d) A schematic view of the carriers' distributions just after the excitation and after hole transfer happening.

benefits from, or even needs, the application of phase modulation and digital lock-in-like acquisition.

The solar cell was made with inverted architecture ITO/ZnOSG/PM6:Y6/MoO$_3$/Ag. The PM6:Y6 weight ratio of the blend was 1:1.2, and all the details about the fabrication are given in the Supporting Information (S1−S3 of SI). Molecular structures for the tested PM6:Y6 device are shown in Figure 2a, while the external quantum efficiency (EQE) spectrum and the current density−voltage (J-V) curve are shown in Figure 2b and its inset, respectively. The OSC has a remarkable current density of 25.49 mA/cm², 0.835 V of V_{oc}, and 74% of Fill Factor. Note that the final device efficiency was 15.7% a value which is among the highest PCE's reported for this blend.[26] The high short circuit current is attributed to the complementary light absorption of the two components over a wide spectral range as can be seen from the absorption spectra shown in Figure 2c.

In the same figure, we overlap the laser spectrum used for 2DES experiment which is centered at 650 nm wavelength with a broad bandwidth (>100 nm). This spectrum gives access to transitions of both Y6 and PM6 (i.e., in the red and the blue part of the spectrum, respectively), thus enabling the characterization of their joint dynamic interaction, which is the essence of the 2D nature of the technique: something hardly achievable by conventional pump−probe. In this case, the expected absorptive maps should show a positive or negative signal in the coordinates, which correspond to the transitions of the two organic semiconductors. In Figure 2e, we indicate the position in the 2D map of positive signals (i.e., GSB and/or SE) expected in 2DES measurements. In case of individual component excitations for PM6 (1) and Y6 (5), GSB signals are expected along the diagonal. In contrast, at the donor/acceptor interface, we can expect three most probable photoinduced interaction processes by considering the energies of the molecule states: electron transfer (2) or exciton transfer (3) from PM6 to Y6 and hole transfer (4) from Y6 to PM6. From a 2DES perspective, processes (2) and (3) would generate a positive signal on the lower cross-peak, because in both cases, the population of Y6 would be affected by these processes. Process (4) would induce a GSB signal at

higher cross-peak because of the removal of electrons from PM6 ground state after excitation of Y6.

Experimental 2DES absorptive maps and their evolution along population time, t_2, are shown in Figure 3a. The diagonal peaks corresponding to the GSB of Y6 and PM6 are centered around 14900 and 16100 cm^{-1} and are consistent with their absorption spectra and the laser spectrum. While the PM6 is excited at its lowest transition, the laser spectrum mainly overlaps with the blue part of Y6 absorption spectrum, generating a partially "hot" exciton in the thin moiety. Yet, the relaxation of the excitons at the bottom of the Y6 band do occur within the laser pulse time window.[32] Notably, t_2 dynamics reveal an increasing GSB signal at upper cross-peak (14900 cm^{-1}, 16100 cm^{-1}). This evolution can be appreciated in the decay associated map (2d-DAS) shown in Figure 3b. The map represents the amplitudes of the exponential decay time of about 1500 fs: result of a global fitting that exploits the variable projection algorithm.[37] The positive and negative amplitudes at diagonal and cross-peak coordinates show an anticorrelated behavior, highlighted by the fitted decays shown in Figure 3c, thus supporting the scenario (4) in Figure 2d that actually the bleaching of the Y6 transition moves toward the PM6 transition. Although a precise estimate of this time constant would require a time window not accessible in this experimental configuration, we can clearly observe a substantial growth of the signal within 1.5 ps.

Such an increase of the upper cross-peak amplitude is seldom observed in 2DES maps of excitonic systems. Conversely, once an exciton is generated, relaxation dominates, thereby increasing below-diagonal signals. Given these considerations, we can safely ascribe the observed signal to an interfacial hole transfer, where a hole localized on a Y6 molecule is transferred to a proximal PM6 unit at the interface (Figure 3d). While the presence and the contribution of hole transfer processes is still debated in the literature, our findings are consistent with recent literature reports, where pump−probe measurements showed that GSB of PM6 is growing in the picosecond range after acceptor excitation.[30] At the same time, it is in contrast with the hypothesis that charge separation happens within the Y6 moiety with subsequent 15 ps hole

transfer to PM6.[32] Notably, the contextual absence of growing GSB or SE signals in the lower cross-peak position indicates that no electron or exciton transfer occurs within 1.5 ps. The absence of the lower cross-peak signal could be also explained by a compensation due to equivalent ESA signal. However, such a coincidence is improbable and is moreover not consistent with literature, where signatures of electron transfer 18 ps have been reported.[32] Then, our results seem to confirm the slower path for electron transfer with respect to the ultrafast hole transfer. The visualization of the signal in 2D-maps helps recognition of correlation between the moiety in which the exciton is generated and the moiety in which the charges move.

In conclusion, our 2DES results show that hole transfer occurs in intermoieties with a 1.5 ps time scale, within the wavelength range of our broadband laser. This work adds another piece in the understanding of efficient hole transfer in low driving force blends in NFAs.

In retrospect, we demonstrated the possibility of unraveling the working mechanism of functioning OSCs by means of a novel 2DES technique based on direct photocurrent detection. This provides an unprecedented level of insight into the excited state dynamics of photovoltaic blends and enables clear identification of the processes driving the efficiency of the cell. Herein, we revealed how ultrafast hole transfer drives the charge generation in PM6:Y6 solar cells, occurring on a time scale of few ps.

In fact, the potential impact of the shown method extends beyond OSCs, and we can envisage its application to the study of hot or multiple carrier dynamics in quantum dots or perovskite solar cells. Moreover, the information extracted from 2DES map, even for the limited energy band and time scan of the current technique, gives direct state-to-state insight on the dynamics in comparison to more standard techniques, such as pump–probe transient absorption, which often need multiple or complementary measurements such as scanning of the pump wavelength. The advantage of local 2DES directly on an operating solar cell, with direct reading of its output, prevents the need for independent preliminary studies on the materials and will spur the development of high-efficiency solar cells.

■ ASSOCIATED CONTENT

ⓢ Supporting Information

The Supporting Information is available free of charge at https://pubs.acs.org/doi/10.1021/acs.jpclett.1c00822.

Cell fabrication, instruments, optical setup and phase modulation (PDF)

■ AUTHOR INFORMATION

Corresponding Authors

Niek F. van Hulst − *ICFO - Institut de Ciencies Fotoniques, The Barcelona Institute of Science and Technology, Barcelona 08860, Spain; ICREA - Institució Catalana de Recerca i Estudis Avançats, Barcelona 08010, Spain;* ⓞ orcid.org/0000-0003-4630-1776; Email: Niek.vanHulst@ICFO.eu

Luca Bolzonello − *ICFO - Institut de Ciencies Fotoniques, The Barcelona Institute of Science and Technology, Barcelona 08860, Spain;* ⓞ orcid.org/0000-0003-0893-5743; Email: Luca.Bolzonello@ICFO.eu

Authors

Francisco Bernal-Texca − *ICFO - Institut de Ciencies Fotoniques, The Barcelona Institute of Science and Technology, Barcelona 08860, Spain*

Luis G. Gerling − *ICFO - Institut de Ciencies Fotoniques, The Barcelona Institute of Science and Technology, Barcelona 08860, Spain*

Jana Ockova − *ICFO - Institut de Ciencies Fotoniques, The Barcelona Institute of Science and Technology, Barcelona 08860, Spain*

Elisabetta Collini − *Dipartimento di Scienze Chimiche, Università degli Studi di Padova, Padova 35131, Italy;* ⓞ orcid.org/0000-0002-1019-9100

Jordi Martorell − *ICFO - Institut de Ciencies Fotoniques, The Barcelona Institute of Science and Technology, Barcelona 08860, Spain; Departament de Física, Universitat Politècnica de Catalunya, Terrassa 08222, Spain;* ⓞ orcid.org/0000-0002-8762-1162

Complete contact information is available at:
https://pubs.acs.org/10.1021/acs.jpclett.1c00822

Notes
The authors declare no competing financial interest.

■ ACKNOWLEDGMENTS

■ REFERENCES

(1) Bránczyk, A. M.; Turner, D. B.; Scholes, G. D. Crossing Disciplines - A View on Two-Dimensional Optical Spectroscopy. *Ann. Phys.* **2014**, *526* (1−2), 31−49.

(2) Scholes, G. D.; Rumbles, G. Excitons in Nanoscale Systems. *Nat. Mater.* **2006**, *5* (11), 920.

(3) Meneghin, E.; Volpato, A.; Cupellini, L.; Bolzonello, L.; Jurinovich, S.; Mascoli, V.; Carbonera, D.; Mennucci, B.; Collini, E. Coherence in Carotenoid-to-Chlorophyll Energy Transfer. *Nat. Commun.* **2018**, *9* (1), 3160.

(4) Zimanyi, E. N.; Silbey, R. J. Unified Treatment of Coherent and Incoherent Electronic Energy Transfer Dynamics Using Classical Electrodynamics. *J. Chem. Phys.* **2010**, *133* (14), 144107.

(5) Righetto, M.; Bolzonello, L.; Volpato, A.; Amoruso, G.; Panniello, A.; Fanizza, E.; Striccoli, M.; Collini, E. Deciphering Hot- and Multi-Exciton Dynamics in Core-Shell QDs by 2D Electronic

Spectroscopies. *Phys. Chem. Chem. Phys.* **2018**, *20* (27), 18176–18183.

(6) Bolzonello, L.; Fassioli, F.; Collini, E. Correlated Fluctuations and Intraband Dynamics of J-Aggregates Revealed by Combination of 2DES Schemes. *J. Phys. Chem. Lett.* **2016**, *7* (24), 4996–5001.

(7) Halpin, A.; Johnson, P. J. M.; Tempelaar, R.; Murphy, R. S.; Knoester, J.; Jansen, T. L. C.; Miller, R. J. D. Two-Dimensional Spectroscopy of a Molecular Dimer Unveils the Effects of Vibronic Coupling on Exciton Coherences. *Nat. Chem.* **2014**, *6* (3), 196–201.

(8) Fuller, F. D.; Ogilvie, J. P. Experimental Implementations of Two-Dimensional Fourier Transform Electronic Spectroscopy. *Annu. Rev. Phys. Chem.* **2015**, *66* (1), 667–690.

(9) Kühn, O.; Mančal, T.; Pullerits, T. Interpreting Fluorescence Detected Two-Dimensional Electronic Spectroscopy. *J. Phys. Chem. Lett.* **2020**, *11* (3), 838–842.

(10) Tekavec, P. F.; Lott, G. A.; Marcus, A. H. Fluorescence-Detected Two-Dimensional Electronic Coherence Spectroscopy by Acousto-Optic Phase Modulation. *J. Chem. Phys.* **2007**, *127* (21), 214307.

(11) Nardin, G.; Autry, T. M.; Silverman, K. L.; Cundiff, S. T. Multidimensional Coherent Photocurrent Spectroscopy of a Semiconductor Nanostructure. *Opt. Express* **2013**, *21* (23), 28617.

(12) Karki, K. J.; Widom, J. R.; Seibt, J.; Moody, I.; Lonergan, M. C.; Pullerits, T.; Marcus, A. H. Coherent Two-Dimensional Photocurrent Spectroscopy in a PbS Quantum Dot Photocell. *Nat. Commun.* **2014**, *5* (1), 5869.

(13) Roeding, S.; Brixner, T. Coherent Two-Dimensional Electronic Mass Spectrometry. *Nat. Commun.* **2018**, *9* (1), 2519.

(14) Aeschlimann, M.; Brixner, T.; Fischer, A.; Kramer, C.; Melchior, P.; Pfeiffer, W.; Schneider, C.; Strüber, C.; Tuchscherer, P.; Voronine, D. V. Coherent Two-Dimensional Nanoscopy. *Science (Washington, DC, U. S.)* **2011**, *333*, 1723–1727.

(15) Tiwari, V.; Matutes, Y. A.; Gardiner, A. T.; Jansen, T. L. C.; Cogdell, R. J.; Ogilvie, J. P. Spatially-Resolved Fluorescence-Detected Two-Dimensional Electronic Spectroscopy Probes Varying Excitonic Structure in Photosynthetic Bacteria. *Nat. Commun.* **2018**, *9* (1), 4219.

(16) Goetz, S.; Li, D.; Kolb, V.; Pflaum, J.; Brixner, T. Coherent Two-Dimensional Fluorescence Micro-Spectroscopy. *Opt. Express* **2018**, *26* (4), 3915.

(17) Bakulin, A. A.; Silva, C.; Vella, E. Ultrafast Spectroscopy with Photocurrent Detection: Watching Excitonic Optoelectronic Systems at Work. *J. Phys. Chem. Lett.* **2016**, *7* (2), 250–258.

(18) Zhang, G.; Zhao, J.; Chow, P. C. Y.; Jiang, K.; Zhang, J.; Zhu, Z.; Zhang, J.; Huang, F.; Yan, H. Nonfullerene Acceptor Molecules for Bulk Heterojunction Organic Solar Cells. *Chem. Rev.* **2018**, *118* (7), 3447–3507.

(19) Liu, J.; Chen, S.; Qian, D.; Gautam, B.; Yang, G.; Zhao, J.; Bergqvist, J.; Zhang, F.; Ma, W.; Ade, H.; et al. Fast Charge Separation in a Non-Fullerene Organic Solar Cell with a Small Driving Force. *Nat. Energy* **2016**, *1* (7), 16089.

(20) Li, S.; Liu, W.; Li, C.-Z.; Shi, M.; Chen, H. Efficient Organic Solar Cells with Non-Fullerene Acceptors. *Small* **2017**, *13* (37), 1701120.

(21) Benatto, L.; Marchiori, C. F. N.; Moyses Araujo, C.; Koehler, M. Molecular Origin of Efficient Hole Transfer from Non-Fullerene Acceptors: Insights from First-Principles Calculations. *J. Mater. Chem. C* **2019**, *7* (39), 12180–12193.

(22) Yuan, J.; Zhang, Y.; Zhou, L.; Zhang, G.; Yip, H. L.; Lau, T. K.; Lu, X.; Zhu, C.; Peng, H.; Johnson, P. A.; et al. Single-Junction Organic Solar Cell with over 15% Efficiency Using Fused-Ring Acceptor with Electron-Deficient Core. *Joule* **2019**, *3* (4), 1140–1151.

(23) Zhang, Z.; Zhang, Z.; Yu, Y.; Zhao, B.; Li, S.; Zhang, J.; Tan, S. Non-Conjugated Polymers as Thickness-Insensitive Electron Transport Materials in High-Performance Inverted Organic Solar Cells. *J. Energy Chem.* **2020**, *47*, 196–202.

(24) Huang, Z.; Ouyang, D.; Ma, R.; Wu, W.; Roy, V. A. L.; Choy, W. C. H. A General Method: Designing a Hypocrystalline Hydroxide Intermediate to Achieve Ultrasmall and Well-Dispersed Ternary Metal Oxide for Efficient Photovoltaic Devices. *Adv. Funct. Mater.* **2019**, *29* (45), 1904684.

(25) Cheng, H. W.; Raghunath, P.; Wang, K. L.; Cheng, P.; Haung, T.; Wu, Q.; Yuan, J.; Lin, Y. C.; Wang, H. C.; Zou, Y.; et al. Potassium-Presenting Zinc Oxide Surfaces Induce Vertical Phase Separation in Fullerene-Free Organic Photovoltaics. *Nano Lett.* **2020**, *20* (1), 715–721.

(26) Perdigón-Toro, L.; Zhang, H.; Markina, A.; Yuan, J.; Hosseini, S. M.; Wolff, C. M.; Zuo, G.; Stolterfoht, M.; Zou, Y.; Gao, F.; et al. Barrierless Free Charge Generation in the High-Performance PM6:Y6 Bulk Heterojunction Non-Fullerene Solar Cell. *Adv. Mater.* **2020**, *32* (9), 1906763.

(27) Wen, Z.-C.; Yin, H.; Hao, X.-T. Recent Progress of PM6:Y6-Based High Efficiency Organic Solar Cells. *Surfaces and Interfaces* **2021**, *23*, 100921.

(28) Cui, Y.; Yao, H.; Zhang, J.; Zhang, T.; Wang, Y.; Hong, L.; Xian, K.; Xu, B.; Zhang, S.; Peng, J.; et al. Over 16% Efficiency Organic Photovoltaic Cells Enabled by a Chlorinated Acceptor with Increased Open-Circuit Voltages. *Nat. Commun.* **2019**, *10* (1), 2515.

(29) Hu, H.; Deng, W.; Qin, M.; Yin, H.; Lau, T. K.; Fong, P. W. K.; Ren, Z.; Liang, Q.; Cui, L.; Wu, H.; et al. Charge Carrier Transport and Nanomorphology Control for Efficient Non-Fullerene Organic Solar Cells. *Mater. Today Energy* **2019**, *12*, 398–407.

(30) Chen, Z.; Chen, X.; Qiu, B.; Zhou, G.; Jia, Z.; Tao, W.; Li, Y.; Yang, Y. M.; Zhu, H. Ultrafast Hole Transfer and Carrier Transport Controlled by Nanoscale-Phase Morphology in Nonfullerene Organic Solar Cells. *J. Phys. Chem. Lett.* **2020**, *11* (9), 3226–3233.

(31) Zhong, Y.; Causa', M.; Moore, G. J.; Krauspe, P.; Xiao, B.; Günther, F.; Kublitski, J.; Shivhare, R.; Benduhn, J.; BarOr, E.; et al. Sub-Picosecond Charge-Transfer at near-Zero Driving Force in Polymer:Non-Fullerene Acceptor Blends and Bilayers. *Nat. Commun.* **2020**, *11* (1), 833.

(32) Wang, R.; Zhang, C.; Li, Q.; Zhang, Z.; Wang, X.; Xiao, M. Charge Separation from an Intra-Moiety Intermediate State in the High-Performance PM6:Y6 Organic Photovoltaic Blend. *J. Am. Chem. Soc.* **2020**, *142* (29), 12751–12759.

(33) Mueller, S.; Lüttig, J.; Malý, P.; Ji, L.; Han, J.; Moos, M.; Marder, T. B.; Bunz, U. H. F.; Dreuw, A.; Lambert, C.; et al. Rapid Multiple-Quantum Three-Dimensional Fluorescence Spectroscopy Disentangles Quantum Pathways. *Nat. Commun.* **2019**, *10* (1), 4735.

(34) Draeger, S.; Roeding, S.; Brixner, T. Rapid-Scan Coherent 2D Fluorescence Spectroscopy. *Opt. Express* **2017**, *25* (4), 3259.

(35) Yan, S.; Tan, H. S. Phase Cycling Schemes for Two-Dimensional Optical Spectroscopy with a Pump-Probe Beam Geometry. *Chem. Phys.* **2009**, *360* (1–3), 110–115.

(36) Damtie, F. A.; Wacker, A.; Pullerits, T.; Karki, K. J. Two-Dimensional Action Spectroscopy of Excitonic Systems: Explicit Simulation Using a Phase-Modulation Technique. *Phys. Rev. A: At., Mol., Opt. Phys.* **2017**, *96* (5), 053830.

(37) Volpato, A.; Bolzonello, L.; Meneghin, E.; Collini, E. Global Analysis of Coherence and Population Dynamics in 2D Electronic Spectroscopy. *Opt. Express* **2016**, *24* (21), 24773.